adequately handled power surges and phase shift changes, since these effects occurred regularly at 8:00 A.M. and 4:30 P.M.

The calculations and results indicate that a furnace designed to emphasize the benefits from the nonlinear radiative heat transfer is simple in construction and mode of control and stable in temperature performance. With no controller producing a variation in the input power, the temperatures do not oscillate.

Nomenclature

A = area, sq. ft.
D = diameter of heater coil or heat shield, inches
d = diameter of heater coil or heat shield, feet
F = ratio of radiative flux after change to flux before change of room temperature, $F = (\Delta Q_c + Q_r)/Q_r$
$\mathfrak{F}$ = factor correcting for nonblack nature of radiative heat transfer surfaces
h_c = convective heat transfer coefficient, B.t.u./hr./sq. ft./° F.
N = number of heat shields
Q_r = radiative heat flux, watts or B.t.u./hr.
Q_c = convective heat flux, watts or B.t.u./hr.
Q_H = heat flux from heater, watts or B.t.u./hr.
T = temperature, ° K.
t = temperature, ° F.

Greek Letters

ΔT_1 = change in temperature at surface 1 effected by change in temperature, ΔT_2, at surface 2, ° C.
ΔT_2 = change of temperature at surface 2, ° C.
ΔQ_c = change in convective heat flux resulting from temperature changes ΔT_2 and ΔT_1; $\Delta Q_c = Q_c$ (before) $- Q_c$ (after), watts or B.t.u./hr.
ϵ = emissivity of radiating surface
σ = Stefan-Boltzmann constant, 0.173×10^{-8} B.t.u./sq. ft./hr./° R^4.

Subscripts

a = after ΔT_2 change
b = before ΔT_2 change
c = convective transfer
H = heater
r = radiative transfer
R = room conditions
1, 2, 3, 4 = index indicating heat transfer surface, 1 = heater surface, 2, 3, and 4 = heat shield surfaces

Literature Cited

Biery, J. C., Cushing, C. R., *Nuclear Eng.* **4**, 109–20 (February 1968).
McAdams, W. H., "Heat Transmission," 2nd ed., pp. 59, 60, 241, McGraw-Hill, New York, 1942.

Received for review January 8, 1968
Accepted September 12, 1968

Work performed under the auspices of the U. S. Atomic Energy Commission.

INTERFACIAL SHEAR MEASUREMENT FOR TWO-PHASE GAS-LIQUID FLOW BY MEANS OF PRESTON TUBES

E. JAMES DAVIS[1]
Chemical Engineering Department, Gonzaga University, Spokane, Wash.

Impact tubes installed on the walls of a wind tunnel were used to measure the shear stress distribution along the top and side walls for concurrent air-water stratified flow. By means of a momentum balance on the gas phase the interfacial shear exerted on the liquid film is computed from the shear stress distribution, pressure drop, and average film thickness. The method is compared with other techniques, and the effects of neglecting the side wall shear stress in the calculation of the interfacial shear are determined. Interfacial shear stresses, local wall shear stresses, pressure drop data, and film thickness characteristics are presented and, where possible, compared with literature results. Significant disagreement among values of smooth wall shear stresses and interfacial shear stresses reported in the literature has been found.

Considerable interest has been shown in recent years in the flow of liquid films dragged by a gas stream over a flat surface. The literature on thin film flow is very extensive (Fulford, 1964), and there is ample evidence that in the concurrent flow of liquid and gas phases in conduits the pressure drop can be considerably greater than that for single-phase gas flow at the same rate of gas flow. If the flow is stratified, surface waves play a large part in this increased momentum transfer.

Since the work of Jeffreys (1925) on the formation of water waves by wind, a number of investigators have studied the generation of surface waves by shear flows. Lock (1954), Feldman (1957), Miles (1957, 1959, 1960, 1962), Benjamin (1959), Cohen and Hanratty (1965), and Craik (1966) analyzed the stability of such flows by solving the Orr-Sommerfeld equations subject to various restrictions. Cohen and Hanratty showed that the wave motion receives its energy from pressure variations and shear stress variations at the interface, which result from gas flow fluctuations caused by the waves. Craik found that the tangential stress component at the interface plays a predominant role in the instability of very thin films. These

[1] Present address, Chemical Engineering Department, Clarkson College of Technology, Potsdam, N. Y. 13676

theoretical studies have been complemented by several experimental investigations.

Hanratty and Engen (1957) reported measurements of the gas velocity profile and film thickness for air-water flow in a horizontal channel. They observed the types of liquid surfaces encountered, characterizing them as smooth, two-dimensional waves, squalls or three-dimensional waves, roll waves, and dispersed flow. Ellis and Gay (1959) and Lilleleht and Hanratty (1961a, 1961b) proposed correlations for the interfacial shear in terms of the surface "roughness." Lilleleht and Hanratty and Smith and Tait (1966) obtained the interfacial shear by means of a momentum balance written about that part of the gas phase extending from the position of the maximum gas velocity to the surface of the liquid film. Using this method it is assumed that the gas flow is two-dimensional, and the shear exerted at the side walls is neglected. Ellis and Gay measured the interfacial shear by analysis of the gas velocity profile. Using semiempirical equations for the velocity profile in terms of the von Karman parameters, u^+ and y^+, and assuming that the liquid surface acts as a rough wall to produce a translation of this velocity profile, they computed the interfacial shear from the equation

$$(u + \Delta u)/u_* = 5.6 + 2.4 \log_e y^+ \quad (1)$$

Van Rossum (1959) reported the results of an investigation on the onset of wave formation, atomization, and the average film thicknesses in horizontal two-phase flow, but because his test section had a 1-to-1 aspect ratio, the side walls must have had a very significant effect on the gas-phase profile, and his results should be analyzed in that light. For the 12-to-1 aspect ratio used by Hanratty and co-workers, the neglect of the side wall shear can lead to little error in the calculation of the interfacial shear, and at relatively low gas Reynolds numbers the assumption of two-dimensional flow is satisfactory. For smaller aspect ratios the effects of the side walls are more important, and at the higher gas flow rates and 8-to-1 ratio used by Smith and Tait, the assumption of two-dimensional flow is questionable.

This paper presents the results of experimental work on the pressure drop, interfacial shear, and surface characteristics of the liquid film for horizontal two-phase flow, using impact tubes mounted on the dry walls to provide the wall shear stress distribution from which, with the pressure drop and average film thickness, the interfacial shear is computed by momentum balance on the gas phase. This method of interfacial shear measurement includes the effects of the side walls and provides information on the limitations of the two-dimensional flow assumption.

Theory

Preston (1954) proposed measuring skin friction by means of a Pitot tube or impact tube resting on the surface. Assuming that the inner law

$$u/u_* = f(u_* y/\nu) \quad (2)$$

is valid in a region close to the surface in both fully developed pipe flow and boundary layer flow, and that the functional relationship is the same for both types of flow, he developed the following equation relating the wall shear stress, τ_o, and the pressure difference, ΔP, measured by the impact tube:

$$\log_{10} \frac{\tau_o d^2}{4\rho\nu^2} = A + B \log_{10} \frac{(\Delta P) d^2}{4\rho\nu^2} \quad (3)$$

where constants A and B were obtained by calibration. Preston's constants were -1.396 and 0.875 for A and B, respectively. After some controversy developed over the validity of Preston's method, Head and Rechenberg (1962) tested and compared Preston tube measurements with wall shear measurements made with Stanton tubes both for pipe and boundary layer flows. They confirmed the validity of Preston's method, comparing their results with Preston's and with those of Smith and Walker (1958) and the National Physical Laboratory in England. For lower values of $(\Delta P)d^2/4\rho\nu^2$ their results were in excellent agreement with Preston's equation, but for higher values the National Physical Laboratory (NPL) constants of $A = -1.353$ and $B = 0.875$ fitted the data better.

Patel (1965) made a more extensive study of the Preston tube, comparing the various correlations proposed. Over a wide range of conditions Patel's calibration equation correlates the extensive data available

$$y^* = 0.8287 - 0.1381x^* + 0.1437x^{*2} - 0.0060x^{*3} \quad (4)$$

where

$$x^* = \log_{10} \frac{(\Delta P) d^2}{4\rho\nu^2}$$

and

$$y^* = \log_{10} \frac{\tau_o d^2}{4\rho\nu^2}$$

The simplicity and good accuracy of the Preston tube make it useful for measuring the shear stress distribution at the solid boundaries in two-phase stratified flow. From the wall shear stress distribution, the pressure drop, and the average film thickness, the interfacial shear can be computed by means of a momentum balance on the gas phase. Figure 1 is a schematic diagram of a channel through which the two phases flow. For a unit length of conduit the momentum balance is

$$\int_{-W/2}^{W/2} \tau_o dz + 2 \int_{\bar{h}}^{H} \tau_s dy + \tau_i W = (\Delta P/L)(H - \bar{h}) \quad (5)$$

where τ_o and τ_s are functions of position along the top and sides of the channel, respectively. The integrals in the momentum balance can be evaluated from local shear stress data by curve-fitting the experimental data and integrating the resulting shear stress distributions.

Experimental

Wall shear, pressure drop, liquid film thickness, and other fluid mechanical parameters were measured in a 20-foot-long Plexiglas wind tunnel, 10 inches wide and 1.028 inches high. The channel (Figure 1) was connected to a convergent sheet metal section which was used as a Venturi to measure the rate of gas flow. Air was supplied by a turbocompressor, passed through a spray chamber where it was cooled and saturated, and entered the test section through the converging section. Preston tubes were placed on the walls of the channel at the positions indicated in the diagram, and a traversing impact tube was installed to measure the gas velocity profile in a vertical plane near the center of the channel, about 16 feet from the inlet to the tunnel. The various pressure differences were measured with micromanometers. Figure 2 shows the method of installing the impact tubes. To verify that the measured shear stress does not depend on the tube diameter two sizes of stainless steel tubes were used, $^1/_8$- and $^1/_{16}$-inch o.d.

The liquid phase, water, was introduced from a constant head tank, passed through a rotameter, and entered the tunnel through perforations in the bottom of the tunnel 6 inches downstream from the test section inlet. At the end of the test section the water was collected in a receiving drum and recycled to the constant head tank. Both the air inlet and the water lines were connected to flexible rubber sections to minimize rippling and waves induced by vibration of the pump or blower.

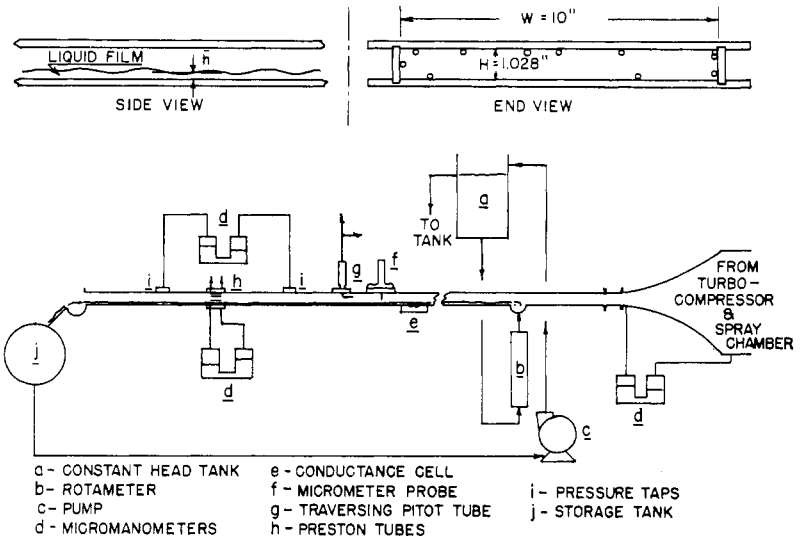

Figure 1. Experimental facility

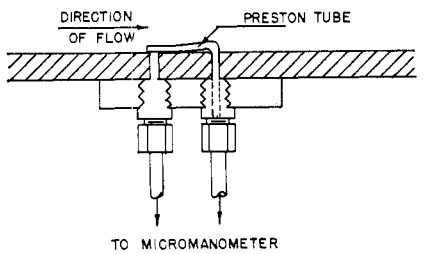

Figure 2. Installation of Preston tubes

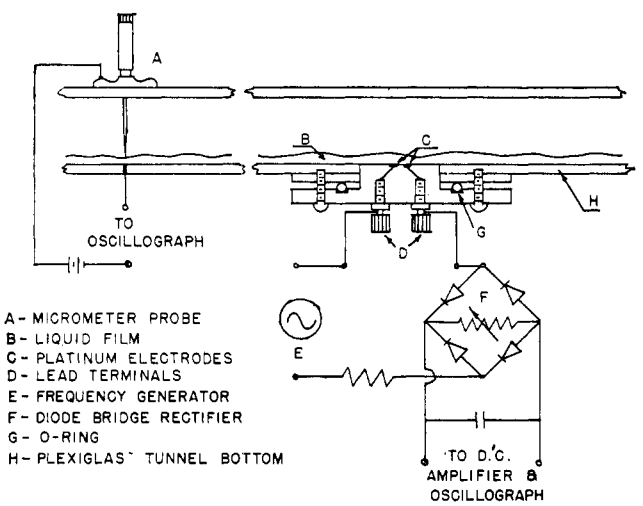

Figure 3. Devices for film thickness measurement

To measure film thicknesses two techniques were applied. A conductance probe attached to a micrometer and wired to a simple circuit (Figure 3) was used in the way McManus (1961) used the conductance probe to measure maximum and minimum film thicknesses. Also shown in Figure 3 is the design of a conductivity cell, consisting of two platinum electrodes installed flush with the tunnel bottom, which was used to measure the instantaneous film thickness. The various methods used to measure film thicknesses have been widely discussed and criticized (Hewitt *et al.*, 1962; Silvestri, 1964), and, although the electrical conductance technique involves some averaging of the film thickness, the electrode size and spacing can be varied to minimize the averaging by designing interchangeable electrodes. The electrodes were installed flush with the flat surface of a cylindrical plug which fitted snugly into the bottom of the tunnel. For thicker films ($h > 0.06$ inch) and films involving roll waves, a cell with an electrode spacing of $^1/_4$ inch (center-to-center) was used. For thinner films and films involving three-dimensional waves, a $^1/_8$-inch electrode spacing was used.

The range of film thicknesses which produces a linear response from the system depends upon the electrode spacing, so each configuration was used over a limited range. The technique is not satisfactory for measurements involving relatively thick films with short wavelength surface waves, for the greater electrode spacing required produces excessive averaging.

The conductivity cell was calibrated in place after each run by varying the thickness of a smooth film flowing over the cell, recording the output on an oscillograph, and comparing the results with measurements using the probe. Some error is involved in the probe measurements, because air flow around the tip causes a slight depression in the liquid film at the higher air flow rates. For the conditions studied, the error is less than 0.002 inch.

Results

The Preston tubes were calibrated by measuring the pressure drop and local shear stresses for single-phase air flow over a wide range of flow rates. For single-phase flow the momentum balance becomes

$$2\int_{-W/2}^{W/2} \tau_o dz + 2\int_0^H \tau_s dy = (\Delta P/L)H \qquad (6)$$

Preston tubes were installed on the bottom of the tunnel for some single-phase flow tests, as shown in Figure 1, to examine the symmetry of the shear stress distribution, and three tubes were installed 29 inches upstream from the main battery of tubes to test for fully developed shear stress profiles. Both fully developed flow conditions and symmetry occurred.

Assuming symmetry about the center line on the tunnel top and bottom, the shear stresses along the horizontal surfaces for each run were curve-fitted by the method of least squares to either a second-degree polynomial

$$\tau_o = a + b\zeta + c\zeta^2 \qquad (7)$$

or a logarithmic equation

$$\tau_o = C_1 + C_2 \log_e \zeta' \qquad (8)$$

where ζ' is the position measured from the edge of the channel, and ζ is the position measured from the center line of the

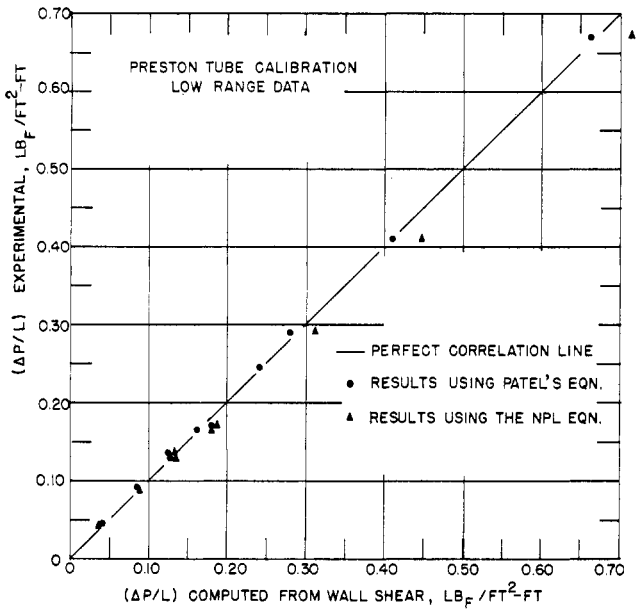

Figure 4. Results of Preston tube calibration

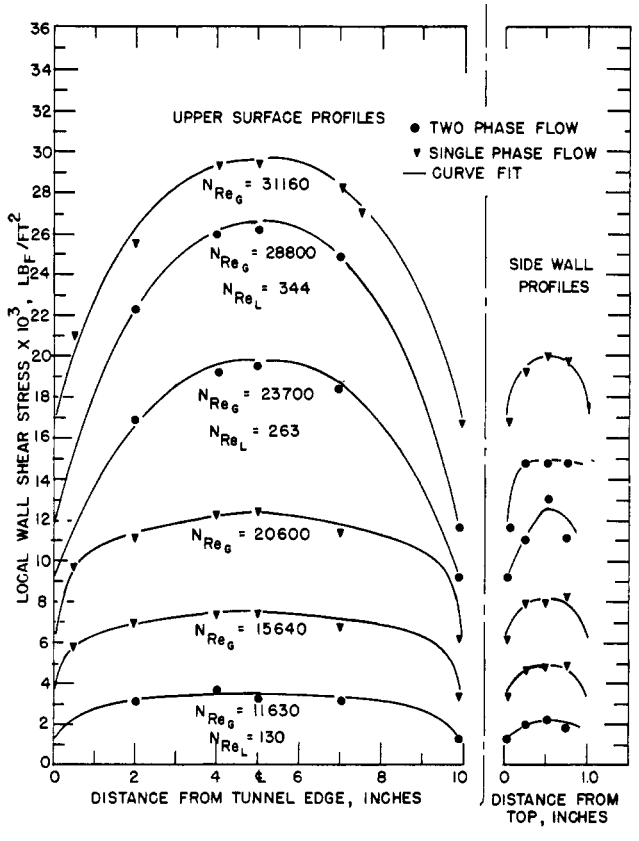

Figure 5. Wall shear stress distributions

wall. For $N_{Re_G} > 21{,}000$, Equation 7 fits the data very well, and for $N_{Re_G} < 21{,}000$, Equation 8 applies. The side wall shear stresses for each run were fitted to a second-degree polynomial, assuming symmetry for single-phase flow.

The left-hand side of Equation 6 was evaluated by integrating the appropriate shear stress distributions over the horizontal and vertical surfaces involved, and the pressure drop per unit length was computed from Equation 6 for each calibration run. The computed pressure drop was compared with the measured pressure drop to test the Preston tubes and evaluate the accuracy of the technique. Figure 4 compares the calculated and experimental pressure drops per unit length for the low range of shear stress data. The results obtained using Patel's correlation (Equation 4) for the Preston tube calibration are in very good agreement with the measured pressure drop per unit length. For the range shown in Figure 4 the average deviation is 2.5%. The results obtained using the National Physical Laboratory calibration are presented for comparison; they are in less satisfactory agreement with the experimental data. For $x^* > 5.6$ Equation 4 overpredicts the shear stress, in agreement with Patel's findings. For the higher range of x^* the Preston tube data were correlated by the equation

$$y^* = -1.458 + 0.875x^* \tag{9}$$

At the higher flow rates involved, the data from the Preston tubes are more scattered, and the average deviation of the computed pressure drop from the experimental pressure drop is 6.7%.

Typical shear stress distributions encountered in both single-phase flow and two-phase flow are shown in Figure 5 for various Reynolds numbers. The Reynolds numbers are defined as follows:

Single-phase flow. $N_{Re_G} = H\bar{U}/\nu_G$

Two-phase flow. $N_{Re_G} = (H - \bar{h})\bar{U}/\nu_G$;

$$N_{Re_L} = Q_L/W\nu_L$$

There are no significant differences in the shear stress profiles between single-phase flow and two-phase flow at the same Reynolds numbers, but the shape of the profiles changes from very flat at $N_{Re_G} = 11{,}630$ to parabolic at $N_{Re_G} = 31{,}160$. These results indicate that for the aspect ratio of 10 to 1 studied here the flow field is not two-dimensional for $N_{Re_G} > 21{,}000$ except, perhaps, over 20% of the tunnel near the center. Except for the effect of the side walls on the flow field, the side walls do not greatly affect the accuracy of the calculation of the interfacial shear. For the range of gas-phase Reynolds numbers studied here ($10{,}000 \leq N_{Re_G} \leq 62{,}400$), the neglect of the side wall shear stress in Equation 5 leads to an overestimate of the average interfacial shear stress by at most 10%. At the higher gas-phase Reynolds numbers, the error is even less. If the method of Hanratty and Engen is used to obtain the interfacial shear, the error involved in neglecting the side wall shear is even less, because the momentum balance is then taken around that part of the gas phase extending from the point of zero shear stress to the surface of the liquid. Of more importance than the magnitude of the side wall shear, however, is the fact that the flow field is not two-dimensional at the higher gas-phase Reynolds numbers. Many of the interfacial shear data in the literature are for systems with aspect ratios lower than 10 to 1 and for relatively high Reynolds numbers, so it is important to examine the effects of the side walls.

To establish the magnitude of the error involved in the measurement of the average interfacial shear from velocity profile measurements, data were obtained on the position of the maximum gas velocity, pressure drop, and average film thickness, and compared with interfacial shear stresses obtained from the wall shear stress distribution by the method outlined above. To define the range and types of conditions studied it is convenient to plot representative runs on the interfacial pattern map of Smith and Tait. Figure 6 shows the surface conditions encountered by Smith and Tait as regions on a plot of

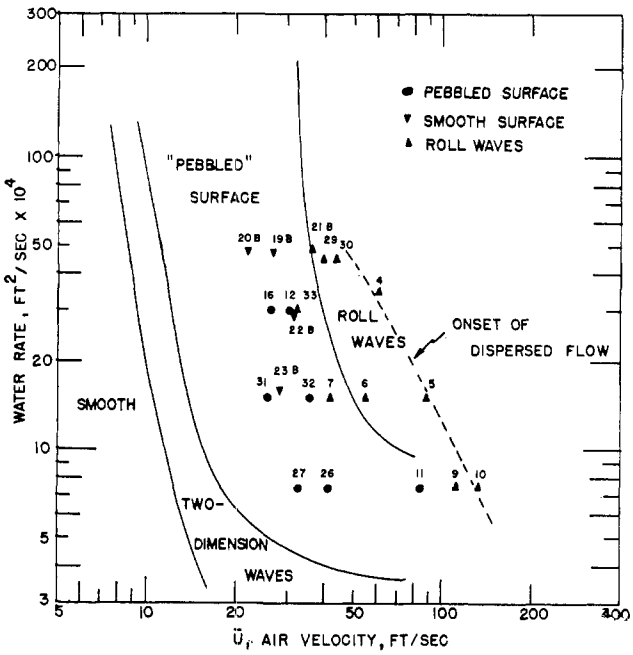

Figure 6. Interfacial structure in air-water flow

water rate (volumetric flow rate per unit width of tunnel) *vs.* the mean air velocity. The solid lines of Smith and Tait should probably be considered to be broader bands marking the transition from one surface type to another. The points indicate the surface conditions observed for some of the runs involved in the present work. The transition from a "pebbled" surface to roll waves was observed to occur at slightly lower air velocities than reported by Smith and Tait, but the general outlines of the map and data agree. The transition from a smooth or two-dimensional wave surface to the pebbled surface occurred at higher velocities than reported by Smith and Tait, and this transition is greatly influenced by the presence of a wetting agent in the liquid. Runs 19B to 23B were made with the addition of a commercial wetting agent to the liquid. For the first two and last two runs smooth surfaces were observed, and for run 21B roll waves were observed. In this work the liquid Reynolds number was varied from 57 to 438.

Runs 4, 5, 10, and 30 were observed to be very near the onset of dispersed flow, for a slight increase in the gas flow rate caused droplets to break from the liquid surface and settle on the tunnel walls, Pitot tube, and Preston tubes. Smith and Tait identified the onset of dispersed flow with the onset of unsteady waves, and at higher liquid flow rates the data in Figure 6 hint that this might be true.

Figure 7 shows representative samples of the oscillograph tracings for runs exhibiting pebbled and roll wave surfaces. Run 33, taken at the onset of roll wave formation, shows the pebbled surface on an underlying roll wave structure. Run 32 is below the onset of roll waves and is characteristic of the pebbled surface runs. Run 7 involved thinner films with very large amplitude and very unsteady roll waves, and run 8 is just at the onset of roll wave formation. The distances between the large peaks of runs 33 and 7 in Figure 7 are in the order of 2 to 3 feet, so the vertical scale is greatly amplified and the waves are greatly distorted in these tracings.

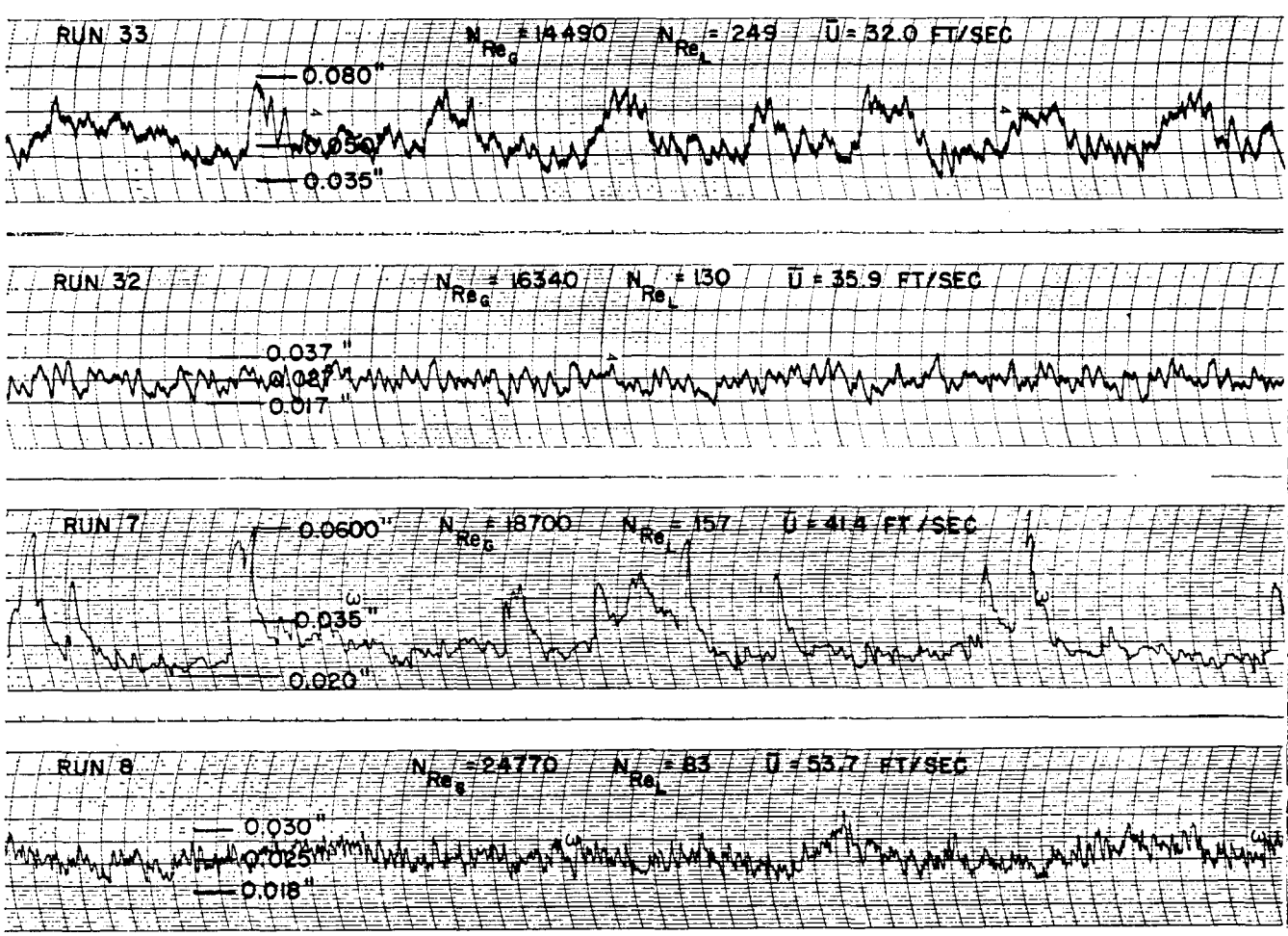

Figure 7. Film thicknesses for air-water two-phase flow

Table I. Interfacial Shear Data

Investigator	*Run No.*	N_{Re_G}	N_{Re_L}	τ_o, *Lb.f/Sq. Ft.*	τ_i, *Lb.f/Sq. Ft.*	f_o	f_i
H-E[a]	54	19,200	127	0.00852	0.0117	0.0023	0.0031
	14	14,250	170	0.00661	0.00787	0.0030	0.0035
	55	12,800	508	0.00562	0.0107	0.0029	0.0053
	56	13,900	508	0.00623	0.0116	0.0028	0.0050
Present	20	10,930	117	0.00318	0.00402	0.00279	0.00352
	31	11,630	130	0.00306	0.00397	0.00230	0.00291
	32	16,340	130	0.00693	0.00793	0.00258	0.00295
	6	26,330	150	0.01853	0.0248	0.00290	0.00388
	7	18,700	157	0.00962	0.0112	0.00269	0.00314
	5	41,100	166	0.0473	0.0602	0.00289	0.00368
	28	15,990	438	0.00673	0.0102	0.00233	0.00355
	21B	17,040	402	0.00850	0.00850	0.00300	0.00300
	29	19,010	427	0.0104	0.0176	0.00250	0.00418
	30	21,030	419	0.0134	0.0230	0.00266	0.00464

[a] *Hanratty and Engen.*

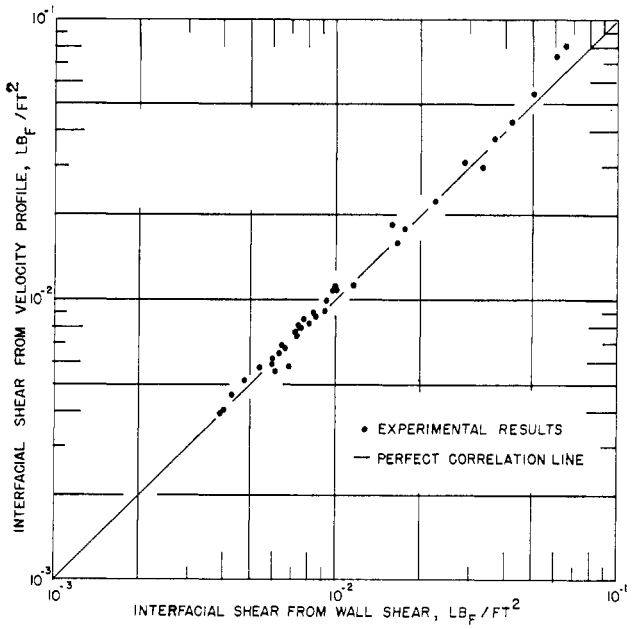

Figure 8. Comparison of methods of interfacial shear measurement

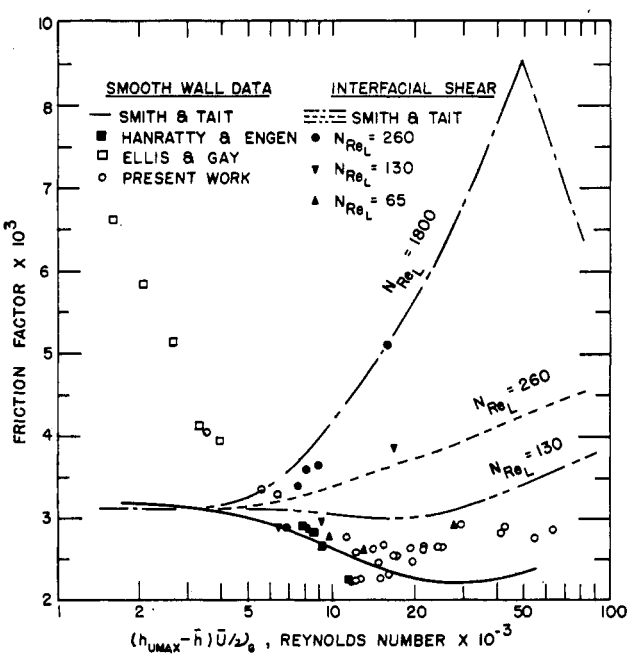

Figure 9. Comparison of interfacial shear stresses and smooth wall shear stresses obtained by various investigators

Figure 8 compares the average interfacial shear stress measured by the method of Hanratty and Engen with the interfacial shear obtained from the wall shear stress distribution. The interfacial shear stresses obtained from the velocity profile data are, as expected, larger than those computed from the wall shear data. For runs with $N_{Re_G} < 20{,}000$ the two methods are in good agreement, and the average deviation is 4.7%. At higher gas-phase Reynolds numbers the interfacial shear obtained from the position of the maximum gas velocity averages 9.4% higher than that computed from the wall shear stress distribution, and individual runs involve errors as large as 23.5%. For lower aspect ratios and similar Reynolds numbers the errors may be even greater.

The literature contains considerable data on interfacial shear in horizontal two-phase flow, but only the work of Smith and Tait (1966) covers a wide range of gas and liquid flow rates to permit suitable comparison. Ellis and Gay (1959) studied the ranges $3000 < N_{Re_G} < 8000$ and $1820 < N_{Re_L} < 3220$, and Hanratty and Engen (1957) reported some interfacial shear values for $N_{Re_G} < 19{,}200$ and $N_{Re_L} < 508$. Table I indicates that the present data and those of the latter investigators are in reasonable agreement over the narrow range involved. Figure 9 compares smooth wall shear stress data and interfacial shear data for various investigations. Since Smith and Tait defined the gas-phase Reynolds number in terms of the position of the maximum velocity of the gas stream, the data are plotted in this form. For the smooth wall data the gas-phase Reynolds number is given by $(H - h_{u\max})\bar{U}/\nu_G$, and for the interfacial shear data the gas-phase Reynolds number is $(h_{u\max} - \bar{h})\bar{U}/\nu_G$.

The smooth wall data, written in terms of the friction factor $f_o = \tau_o g_c/\rho_G \bar{U}^2$, are plotted against the former Reynolds number for the figure. The data of Ellis and Gay, Hanratty and Engen, and the present work are in good agreement for $N_{Re_G}{}^* < 12{,}000$, which is the limit of the data available from these investigators, but the Smith and Tait results are in very substantial disagreement for $N_{Re_G}{}^* < 8000$. Only in the range $8000 < N_{Re_G}{}^* < 16{,}000$ are the Smith and Tait values in agreement with other data. Although van Rossum (1959) reported smooth wall shear stress data, his results are not comparable with the results of the investigators indicated because of the different flow field involved in his tunnel of square cross section. The smooth wall data from the present work are based on the average wall shear stress for the upper surface of the tunnel for both single-phase and two-phase flow, and the average shear stress was computed from the shear stress distribution for that surface.

In Figure 9 the interfacial shear data are presented in terms of the interfacial friction factor defined by $f_i = \tau_i g_c/\rho_G \bar{U}^2$. The

extensive data of Smith and Tait (1966) are indicated by lines drawn through their data, and their data points are not included. Representative data points from the present work for three different liquid-phase Reynolds numbers and various gas-phase Reynolds numbers are plotted for comparison. At the lowest liquid-phase Reynolds numbers, $N_{Re_L} \leq 65$, the result of Smith and Tait and the present results are in fair agreement, and the friction factors for such thin film flow are the same as those for flow over a smooth wall for $N_{Re_G}{}^* < 15{,}000$. For the higher liquid-phase Reynolds numbers indicated in the figure the agreement is poor, especially for $N_{Re_G}{}^* > 10{,}000$, for the interfacial shear stresses obtained by means of the method proposed here are considerably larger than those measured by Smith and Tait. It is likely that the discrepancy is due to the error involved in the assumption of two-dimensional flow by the latter investigators. In terms of the gas-phase Reynolds number defined previously, an $N_{Re_G}{}^*$ of 10,000 corresponds to approximately 20,000, and above this value it has been shown that the deviations from a flat wall shear stress profile are considerable.

Conclusions

The method of interfacial shear measurement proposed and used here to obtain the interfacial shear for horizontal air-water flow is an accurate and reliable technique. Because of the significant deviations from two-dimensional flow that occur in rectangular test sections of finite aspect ratio at higher gas phase Reynolds numbers, the method is more accurate than other techniques proposed, for it takes into account the effects of the side walls.

Acknowledgment

The author is grateful to the National Science Foundation for grant GK801 and to the Petroleum Research Fund of the American Chemical Society for grant 978B for two-phase flow research. He is most appreciative of the assistance given by B. J. Allen, who obtained many of the data used, and by M. J. Duffy, who developed some of the experimental techniques.

Nomenclature

a = constant in Equation 7
A = constant in Equation 3
b = constant in Equation 7
B = constant in Equation 3
c = constant in Equation 7
C_1 = constant in Equation 8
C_2 = constant in Equation 8
d = Preston tube diameter
f_i = $\tau_i g_c/\rho_G \bar{U}^2$, interfacial friction factor
f_o = $\tau_o g_c/\rho_G \bar{U}^2$, smooth wall friction factor
g_c = conversion factor
$\bar{h}$ = average film thickness, inch
h_{umax} = position of maximum gas velocity
H = height of wind tunnel
L = length
N_{Re_G} = $(H - \bar{h})\bar{U}/\nu_G$, gas-phase Reynolds number
N_{Re_L} = $Q_L/W\nu_L$, liquid phase Reynolds number
$N_{Re_G}{}^*$ = $\left\{\begin{matrix}(H - h_{umax})\bar{U}/\nu_G \\ (h_{umax} - \bar{h})\bar{U}/\nu_G\end{matrix}\right\}$ gas-phase Reynolds numbers
ΔP = pressure difference
Q_L = liquid volumetric flow rate
Δu = velocity profile shift
u^+ = u/u_*, dimensionless velocity
u_* = $\sqrt{\tau g_c/\rho}$, friction velocity
$\bar{U}$ = mean velocity of gas phase, ft./sec.
W = tunnel width
x^* = $\log_{10} (\Delta P)d^2/4\rho\nu^2$, group of variables in Equation 4
y = vertical position measured from tunnel bottom
y^+ = yu_*/ν, dimensionless distance
y^* = $\log_{10} \tau_o d^2/4\rho\nu^2$, group of variables in Equation 4
z = horizontal position
ζ = horizontal position measured from center of the tunnel
ζ' = horizontal position measured from edge of tunnel
ν = kinematic viscosity
τ_i = interfacial shear stress
τ_o = wall shear stress
τ_s = side wall shear stress

Literature Cited

Benjamin, T. B., *J. Fluid Mech.* **6,** 161–205 (1959).
Cohen, L. S., Hanratty, T. J., *A.I.Ch.E. J.* **11,** 138–44 (1965).
Craik, A. D. D., *J. Fluid Mech.* **26,** 369–92 (1966).
Ellis, S. R. M., Gay, B., *Trans. Inst. Chem. Engrs.* **37,** 206–13 (1959).
Feldman, S., *J. Fluid Mech.* **2,** 343–70 (1957).
Fulford, G. D., *Advan. Chem. Eng.* **5,** 151–236 (1964).
Hanratty, T. J., Engen, J. M., *A.I.Ch.E. J.* **3,** 299–304 (1957).
Head, R. M., Rechenberg, I., *J. Fluid Mech.* **14,** 1–17 (1962).
Hewitt, G. F., King, R. D., Lovegrove, P. C., Atomic Energy Research Establishment, **AERE R 3921** (1962).
Jeffreys, H., *Proc. Roy. Soc.* **A107,** 189 (1925).
Lilleleht, L. U., Hanratty, T. J., *A.I.Ch.E. J.* **7,** 548–50 (1961a).
Lilleleht, L. U., Hanratty, T. J., *J. Fluid Mech.* **11,** 65–78 (1961b).
Lock, R. C., *Proc. Cambridge Phil. Soc.* **50,** 105–24 (1954).
McManus, H. N., *ASME Publ.* **61-HYD-20** (1961).
Miles, J. W., *J. Fluid Mech.* **3,** 185–204 (1957); **6,** 568 (1959); **8,** 593–610 (1960); **13,** 433–48 (1962).
Patel, V. C., *J. Fluid Mech.* **23,** 185–208 (1965).
Preston, J. H., *J. Roy. Aeronaut. Soc.* **58,** 109 (1954).
Silvestri, M., *Advan. Heat Transfer* **1,** 384–9 (1964).
Smith, D. S., Walker, J. H., Natl. Aeronaut. **NACA TN 4231** (1958).
Smith, T. N., Tait, R. W. F., *Chem. Eng. Sci.* **21,** 63–75 (1966).
van Rossum, J. J., *Chem. Eng. Sci.* **11,** 35–52 (1959).

RECEIVED for review February 14, 1968
ACCEPTED September 19, 1968